Liquid Wells as Self-Healing, Functional Analogues to Solid Vessels

Johannes M. Scheiger, Mariia A. Kuzina, Michael Eigenbrod, Yanchen Wu, Fei Wang, Stefan Heißler, Steffen Hardt, Britta Nestler, and Pavel A. Levkin*

Liquids are traditionally handled and stored in solid vessels. Solid walls are not functional, adaptive, or self-repairing, and are difficult to remove and re-form. Liquid walls can overcome these limitations, but cannot form free-standing 3D walls. Herein, a liquid analogue of a well, termed a "liquid well" is introduced. Water tethered to a surface with hydrophobic–hydrophilic core–shell patterns forms stable liquid walls capable of containing another immiscible fluid, similar to fluid confinement by solid walls. Liquid wells with different liquids, volumes, and shapes are prepared and investigated by confocal and Raman microscopy. The confinement of various low-surface-tension liquids (LSTLs) on surfaces by liquid wells can compete with or be complementary to existing confinement strategies using perfluorinated surfaces, for example, in terms of the shape and height of the confined LSTLs. Liquid wells show unique properties arising from their liquid aggregate state: they are self-healing, dynamic, and functional, that is, not restricted to a passive confining role. Water walls can be easily removed and re-formed, making them interesting as sacrificial templates. This is demonstrated in a process termed water-templated polymerization (WTP). Numerical phase-field model simulations are performed to scrutinize the conditions required for the formation of stable liquid wells.

1. Introduction

Shaped solid objects such as pottery, vases, metal canisters, or glasses have been used to confine, store, and handle liquids throughout human history. In modern times, the manipulation and control of liquids on surfaces without solid walls sparked interest in various applications such as microfluidic devices,[1] lab-on-a-chip,[2–3] repellent coatings,[4] oil–water separation,[5] and miniaturized chemistry or biology.[6–8] A commonly employed strategy is hydrophilic–hydrophobic chemically patterned surfaces, which allow spatial confinement of aqueous compartments.[9–15] Development of omniphobic–omniphilic or superoleophobic patterned substrates made it possible to confine droplets of low-surface-tension liquids (LSTLs) and significantly improved the capabilities of surface-templated liquids.[16] The preparation of omniphobic or superoleophobic surfaces typically requires perfluorinated chemicals for surface modification or lubricant infused surfaces (LISs).[17] However, the use of perfluorinated chemicals is environmentally questionable due to their biopersistence, whereas LISs are often not durable due to partial miscibility of the lubricants in LSTLs.[18–20] Furthermore, these methods often solely constrain the area wetted by the LSTL and there are only a few demonstrations of patterned LSTLs.[21–26] Jokinen

J. M. Scheiger, M. A. Kuzina, Prof. P. A. Levkin
Institute of Biological and Chemical Systems – Functional Materials Systems (IBCS-FMS)
Karlsruhe Institute of Technology (KIT)
Hermann-von-Helmholtz Pl. 1
76344 Eggenstein-Leopoldshafen, Germany
E-mail: levkin@kit.edu
Dr. M. Eigenbrod, Prof. S. Hardt
Mechanical Engineering Department
Institute for Nano- and Microfluidics
Technical University of Darmstadt
Alarich-Weiss-Str. 10, 64287 Darmstadt, Germany

Y. Wu, Dr. F. Wang, Prof. B. Nestler
Institute of Applied Materials – Computational Materials Science
Karlsruhe Institute of Technology (KIT)
Straße am Forum 7, 76131 Karlsruhe, Germany
S. Heißler
Institute of Functional Interfaces (IFG)
Karlsruhe Institute of Technology (KIT)
Hermann-von-Helmholtz-Platz 1, 76344 Eggenstein-Leopoldshafen, Germany
Prof. B. Nestler
Institute of Digital Materials Science
Karlsruhe University of Applied Sciences
Moltkestraße 30, 76133 Karlsruhe, Germany
Prof. P. A. Levkin
Institute of Organic Chemistry (IOC)
Karlsruhe Institute of Technology (KIT)
Fritz-Haber-Weg 6, 76021 Karlsruhe, Germany

et al. demonstrated the use of superhydrophobic–hydrophilic patterns to create designer multiphase droplets to confine an organic liquid droplet inside an aqueous droplet or for miniaturized liquid–liquid–liquid extraction application.[27,28] Other solid-wall-free strategies to confine liquids include embedding of water into a matrix of viscous poly(dimethylsiloxane) oil,[29,30] water–oil emulsions in microfluidic devices,[31,32] and aqueous channels held by immiscible magnetic liquid barriers.[33] With these strategies, however, only water can be confined. Here we demonstrate that on small scales the mechanical stability of water confined on a hydrophilic surface can be high enough to act as a solid-like wall, capable of containing another liquid. Using this strategy, we could create liquid wells containing various LSTLs in different shapes and volumes, with 1-nonanol and n-hexadecane being discussed in most detail. The unique properties of free-standing liquid walls, such as being adaptive, self-restoring, and functional, are demonstrated. For this purpose, we performed experiments such as cutting the wall with a knife or extracting a dye from the confined liquid into the wall. The experimental findings are compared with numerical results obtained from phase field modeling. The ease of removal of the water wall motivated a novel polymerization method, termed "water-templated polymerization" (WTP), in which water acts as a mold to fabricate structured polymer films.

2. Results and Discussion

Water was used as a barrier to confine LSTLs as a liquid analogue of a solid well (**Figure 1**A). The water barrier itself was confined in a hydrophilic surface area surrounded by hydrophobic surface areas, in which the hydrophilic area enclosed a hydrophobic area. Then, an LSTL was deposited to the hydrophobic surface area within the water wall, which spread out and was confined in the shape predetermined by the shape of the water barrier (Figure 1B; Video S1, Supporting Information). "Hydrophilic" and "hydrophobic" surface area refer to surface areas functionalized with 2-mercaptoethanol and 1-dodecanthiol, respectively, thus not making use of fluorochemicals. Information about the surface modification can be found in the Supporting Information (Figures S1, S2, and Table S1, Supporting Information). To demonstrate, that the variety and complexity of shapes obtainable with this core–shell approach is comparable to LSTLs confined by omniphobic–omniphilic surfaces, we created several patterns with varying interior angles (60°, 90°, 120°) and a maze-like structure (Figure 1C).[21,22,24,26] Compartments with an organic layer feature size down to 1 mm were fabricated.

Analyzing the shape of the fluids contained in anisotropic patterns (e.g., rectangular and triangular pattern) revealed that
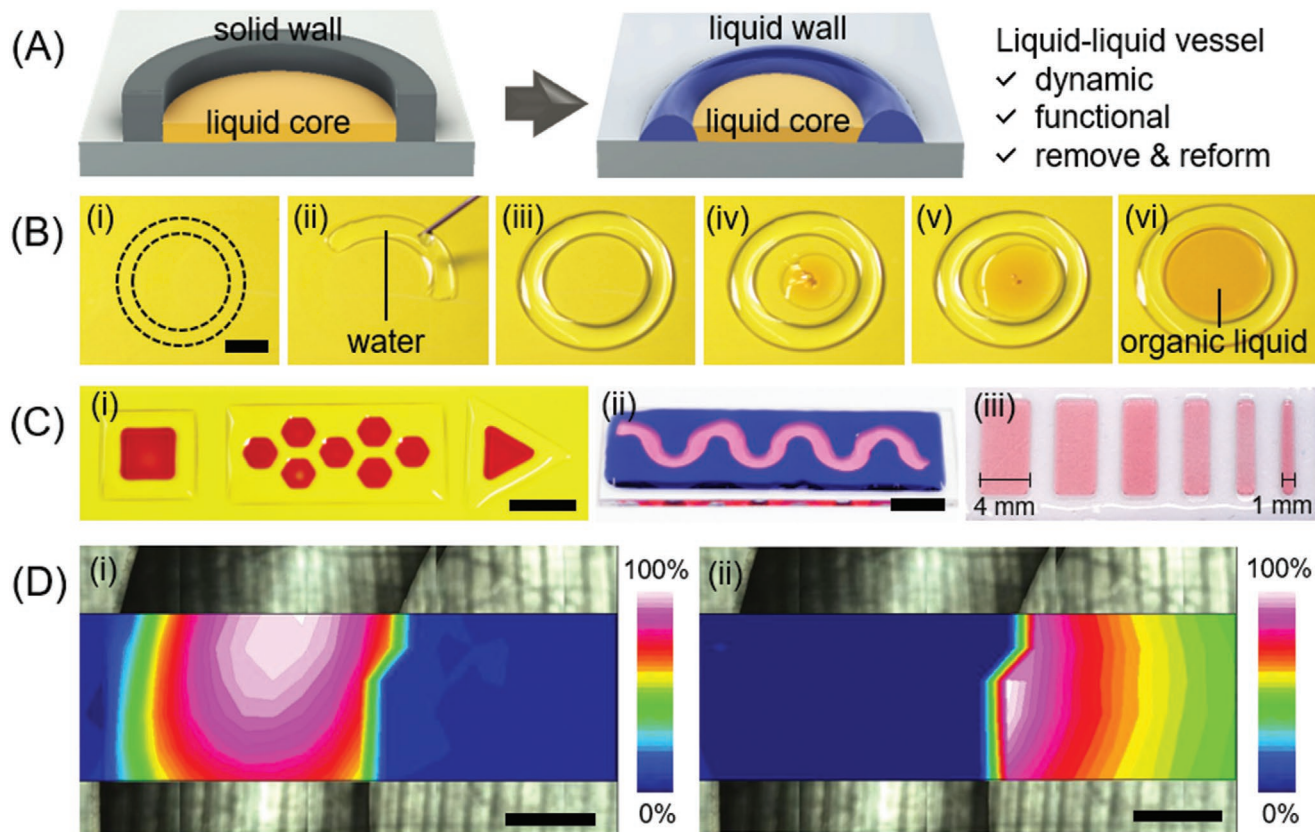

Figure 1. A) Scheme of a liquid contained in a solid vessel (left) and inside liquid water walls, that is, a liquid well (right). B) Formation of a circular liquid well. Water forms a ring on the hydrophilic surface area (dashed line). The organic solvent (1-nonanol, dyed with Oil Red O) is then added into the liquid well. Scalebars: 5 mm. C) Images of liquid wells with various shapes containing different LSTLs. i) Red liquid: toluene dyed with Oil Red O. ii) Blue liquid: water dyed with blue ink; pink liquid: 1-nonanol dyed with Rose Bengal. iii) Transparent liquid: water; pink liquid: 1-nonanol dyed with Rose Bengal. Scalebars: 10 mm. D) Raman map of a ring-shaped liquid well containing 1-nonanol. i,ii) Relative intensities of the O—H stretching vibration (i) and the C—H stretching vibration (ii). Scalebars: 1 mm.

**ADVANCED
SCIENCE NEWS**

www.advancedsciencenews.com

**ADVANCED
MATERIALS**

www.advmat.de

no sharp edges, but instead rounded edges formed (Figure 1C). This is expected, considering that the shapes of the liquid surfaces are governed by the Young–Laplace equation, that is, the minimization of the potential energy under the constraint of conservation of each liquid volume. Accordingly, a retention of shapes was observed for round shapes after the addition of the organic liquid. Thus, the investigation of the liquid–liquid interface was performed with circular patterns, that is, a ring of water as a wall to confine a circular organic core. To verify the chemical composition of the aqueous wall confining an organic core, a chemical map was created along the liquid–liquid interface via Raman spectroscopy (Figure 1D). The shell and core were filled with water and 1-nonanol, respectively. Spectra were measured at different spots of the surface and the Raman scattering intensity of the C−H$_{stretch}$ (3020 to 2780 cm^{-1}) and O−H$_{bend}$ (3100 to 3700 cm^{-1}) vibrations were integrated to visualize the phase-separation of the 1-nonanol and the water phase, respectively. The intensity of the O−H vibration increased toward the middle of the ring, presumably due to an increase in the height of the water layer because of the curvature of the water wall. The opposite was observed for the C−H vibrations in the 1-nonanol phase, which decreased in scattering intensity from the interface toward the center of the circle. Due to the long time (2 h) required for the measurement, LiCl (0.5 mg mL^{-1}) was added to the aqueous phase to reduce evaporation.[34] Full Raman spectra and their position on the surface can be found in the Supporting Information (Figure S3, Supporting Information).

The scope of organic liquids that could be contained within the water walls was elucidated for solvents with different chemical and physical properties (Figure S4 and Table S2, Supporting Information). In brief, liquids miscible with water formed binary solutions with the water walls, which then spread out over the glass substrate (ethanol–water) or remained within the ring-shape of the hydrophilic pattern (tetrahydrofuran–water, N,N′-dimethylformamide–water). In a series of primary alcohols with increasing length of their alkyl chain, that is, ethanol, 1-butanol, 1-nonanol, only the least polar 1-nonanol was confined by the water barrier. Non-polar solvents, such as toluene, dichloromethane, n-hexadecane, n-octane, and n-hexane could be confined. Interestingly, even water droplets could be confined within the water barrier by suppressing their ability to merge with the water wall (Figure S5, Video S2, and Table S3, Supporting Information).

Liquid walls have novel and unique properties distinguishing them from solid vessels. For example, it was observed that liquid wells could contain more liquid inside than we anticipated based on their dimensions. This was enabled by an adaptive deformation of the water wall. To demonstrate the adaptive capacity of the liquid wall, we filled 1-nonanol into a ring-shaped pattern of water (60 µL) and increased the volume of 1-nonanol stepwise from 50, 100, 150 to 200 µL (**Figure 2**A). Increasing the volume of 1-nonanol leads to a visible deformation of the water ring. This enabled the liquid well to contain up to 200 µL of 1-nonanol, which is more than three times
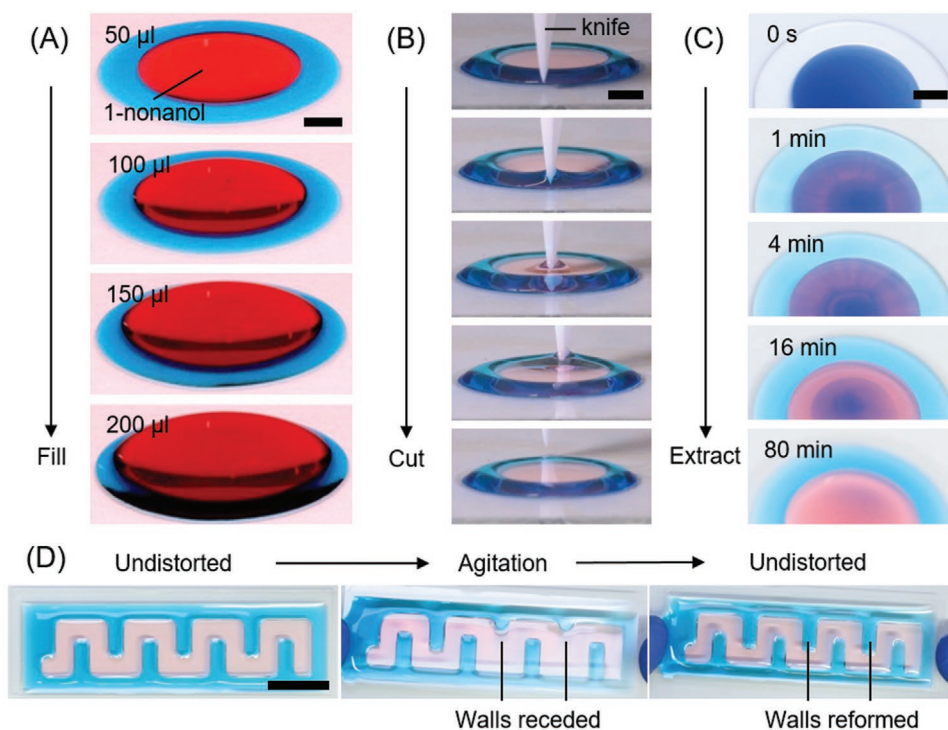

Figure 2. Unique properties of liquid walls. A) Capacity test for 1-nonanol. Up to 200 µL of 1-nonanol were confined by a ring of water (60 µL). The inner and outer diameter of the hydrophilic surface area were 12 and 18 mm, respectively. B) Self-healing properties of the water wall. Despite being cut by a knife, the water wall confining the organic phase re-forms itself. C) Liquid–liquid extraction experiment. A solution of methylene blue (0.1 vol%) and Oil Red O (0.1 vol%) in 1-decanol (30 µL) was deposited inside the water wall (100 µL). Over time, methylene blue diffuses into the aqueous phase, whereas Oil Red O remains in the organic phase. D) Dynamic receding and re-forming of the water wall structure upon agitation. Scalebars (A–C): 5 mm. Scale-bar (D): 15 mm.

ADVANCED
SCIENCE NEWS
www.advancedsciencenews.com

ADVANCED
MATERIALS
www.advmat.de

the volume of the water wall. With 200 µL of 1-nonanol in the liquid well, the meniscus of 1-nonanol was higher than that of the water barrier. In this case, capillary forces balance the gravitational forces on top of the water ring and prevent the organic liquid from escaping. Generally, the capacity of a liquid well is related to the height of the liquid wall surrounding the well. This height is defined by a balance of capillary and gravitational forces, resulting in a length scale of $\lambda_c = (\gamma_{wa}/(\rho_w g))^{1/2}$, termed the capillary length ($\lambda_{c(water)} = 2.73$ mm). In this expression, γ_{wa} is the surface tension of water, ρ_w is the mass density of water and g is the gravitational acceleration. For the case that the radial extension of the liquid wall is much larger than λ_c, the rounded liquid surface will become increasingly flat, and the height of the wall approaches a value of $2\lambda_c \sin(\theta_w/2)$, where θ_w is the contact angle of water on the substrate.[35] To experimentally determine the height limitations of the liquid well, the height of the water wall was measured for increasing volumes of water. A maximum height of 1.95 mm was reached for 210 µL water (Figure S6, Supporting Information). To investigate the influence of a liquid contained inside the well on the height of the water wall, different volumes of 1-decanol were added while keeping the volume of water constant at 60 µL. Addition of 40 µL 1-decanol to the water wall decreased its height from 0.63 to 0.52 mm. Further addition of 1-decanol up to a total volume of 60 µL caused the height of the water wall to increase to 0.58 mm, approaching the initial height without 1-decanol (Figure S6, Supporting Information). The height of the water walls is thus adjustable by their volume, which gives access to facile tuning of the wells capacity. This is different from omniphobic–omniphilic surface patterns, where the height and volume of the confined LSTL critically depend on the contact angle θ_{LSTL} of the LSTL with the omniphobic surface, which is arguably harder to tune dynamically than the height of the liquid wall.[24] The maximum height of a contained liquid in a liquid well was 1.97 ± 0.02 mm for 330 µL of 1-decanol confined by 60 µL water (Figure S6, Supporting Information). As in the case of 1-nonanol (Figure 2A), the height of the 1-decanol meniscus is then exceeding the height of the water wall.

As a Newtonian fluid, water rapidly deforms when exposed to mechanical forces and is inherently self-healing due to its high molecular mobility. To test whether this applies to the liquid walls, a liquid well filled with 1-nonanol was repeatedly cut with a knife (Figure 2B). Both the liquid wall as well as the fluid contained within, that is, the liquid well retained its structural integrity even after several cuts. However, small droplets of 1-nonanol can be moved out of the liquid wall, following the direction of the knife (Figure S7, Supporting Information). The limiting factor for the self-healing of the water wall is thus the stability of the chemical pattern on the surface and not the wall itself, at least when damages with a small Weber number are considered.

Solid containers fulfill a solely confining role, whereas a liquid wall can provide an added value. To explore a potential functionality of the water wall in a liquid well, an extraction experiment was performed (Figure 2C). A dye solution consisting of Oil Red O (0.1 vol%) and methylene blue (0.1 vol%) dissolved in 1-decanol (30 µL) was deposited in a ring of water (100 µL). Immediately after the deposition (0 s) of the dye

solution, methylene blue started to diffuse into the water ring, whereas Oil Red O remained in the 1-decanol phase. After 80 min, the phases were homogenous, and the separation is visible with bare eyes. The water wall can thus extract hydrophilic compounds from the confined organic phase, which could be useful for miniaturized chemistry, sensing, and microfluidics.

It is critically important for any vessel that the liquid inside is not released spontaneously or accidentally upon mild mechanical agitation. To demonstrate that the liquid water walls can retain the confined liquid under non-static conditions, a channel like liquid well was gently shaken and tilted. The inner water walls deformed or even retracted from some areas but re-formed their original state after the system was static again (Figure 2D). Liquid wells thus exhibited a sufficient robustness for convenient use in the laboratory. These experiments show, by simple means, the unique properties arising from using a liquid rather than a solid material to contain another liquid, such as being dynamic, adaptive, self-restoring, and functional. Videos and additional snapshots of the cutting, diffusion, and agitation experiments are available in the Supporting Information (Figure S8 and Videos S3–S5, Supporting Information).

To improve our understanding of the liquid wall–solvent interaction, we investigated the respective interfaces of 1-nonanol or n-hexadecane with water. Differences in the expression of angular shapes of liquid wells containing 1-nonanol or n-hexadecane were visible even with bare eyes. For example, 1-nonanol deposited in a triangular liquid well resulted in the shape of a Reuleaux triangle, whereas the use of n-hexadecane resulted in a barely altered triangular shape (**Figure 3**A). Further, when equal volumes of 1-nonanol or n-hexadecane were deposited in identical water walls, n-hexadecane occupied a larger share of the projected surface area of the total pattern than 1-nonanol, that is, 47% and 37%, respectively (Figure S9, Supporting Information). Thus, the solvent contained in the liquid well strongly influenced the shape of the interface. To elucidate this discrepancy, confocal laser scanning microscopy (CLSM) was used to image the liquid–liquid interface of water with n-hexadecane and 1-nonanol (Figure 3B). The shape of the interface at the hydrophilic and hydrophobic surface boundary was imaged before and after addition of n-hexadecane or 1-nonanol. When n-hexadecane was added, the shape of the water ring barely changed. However, for 1-nonanol the water ring protruded into the space filled with 1-nonanol, which explains the observed difference in occupied space between 1-nonanol and n-hexadecane. Due to the interaction of the organic liquid with the water wall, the height of the organic liquid does not decrease in a continuous, monotonic way as observed for omniphobic–omniphilic patterned surfaces.[21,22,24]

To understand the different shapes obtained at the water–solvent interface and to support the experimental observations, liquid wells were simulated with a phase-field model (**Figure 4**). Coupling the phase-field model with an appropriate boundary condition at the wall can capture the Young's contact angle as well as the so-called Neumann's triangle at a multiple phase junction via minimizing the total free energy of the system. The parameter setups and the phase-field simulations are briefly described in the Supporting Information section. A detailed description of the phase-field model is given by Garcke and co-workers.[36]
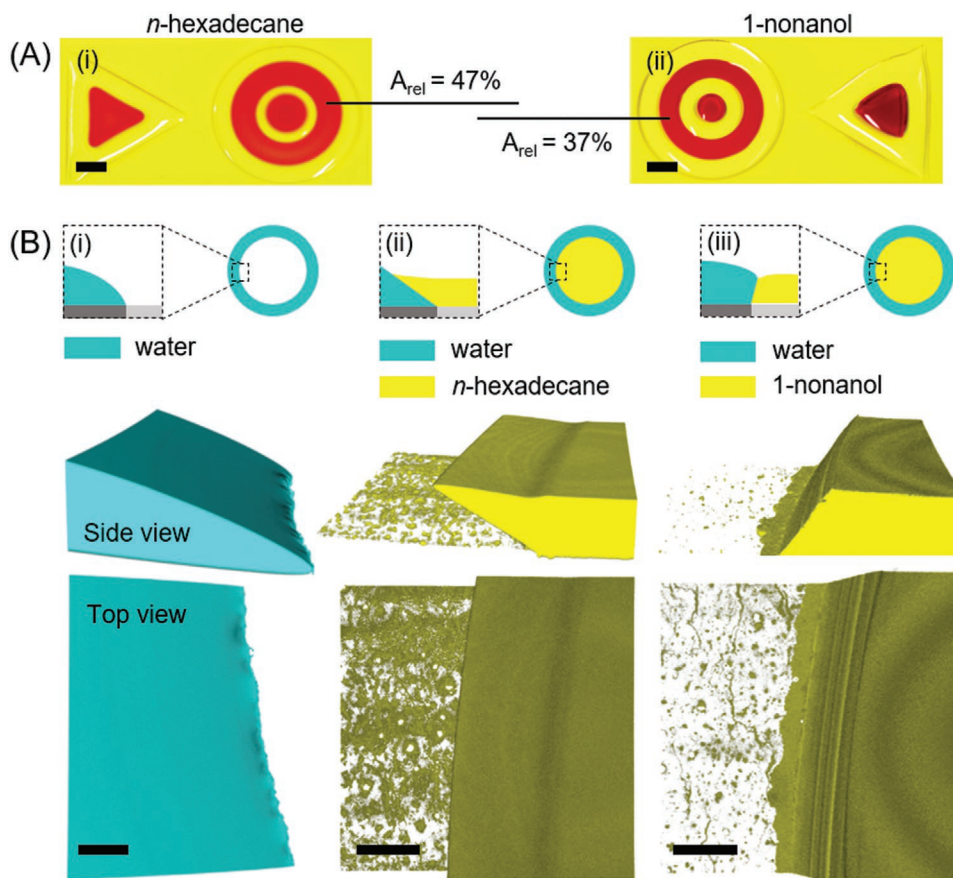
Figure 3. A) Photographs (top view) of triangular and matryoshka liquid wells filled with *n*-hexadecane (i) and 1-nonanol (ii). The organic phases were dyed red with Oil Red O. A_{rel} is the ratio between the projected surface area of the organic phase and the total surface area of the pattern. Scalebar: 5 *mm*. B) CLSM *z*-stack images (side- and top-view) of a water ring at the water–air interface (i), the water–hexadecane interface (ii), and the water–1-nonanol interface (iii). Scalebars: 200 µm.

According to Neumann's triangle rule, the formation of a stable three-phase contact line between an organic liquid, water, and air, is possible if the sum of the surface tensions γ_{oa} (organic liquid–air) and γ_{ow} (organic liquid–water) is greater than γ_{wa} (water–air).[37] It was hypothesized, that the same requirement ($\gamma_{ow} + \gamma_{oa} > \gamma_{wa}$) must be fulfilled to confine an organic liquid by a wall of water. Since the surface tension of the water–air interface is high ($\gamma_{wa} = 72.86$ mN m^{-1}), this is the case for *n*-hexadecane ($\gamma_{oa} = 26.95$ mN m^{-1}, $\gamma_{ow} = 55.3$ mN m^{-1}) but not for 1-nonanol ($\gamma_{oa} = 28.0$ mN m^{-1}, $\gamma_{ow} = 8.8$ mN m^{-1}).[38–40] However, if the Gibbs adsorption isotherm, that is, the change in surface tensions due to the partial solubility of water in 1-nonanol and vice versa (1.76 mol L^{-1} and 1.94 mmol L^{-1}, respectively)[41,42] is considered, the phase-field model is able to predict a confinement as observed experimentally. According to Lee et al., the surface tension of the water–air interface can be reduced from 72.86 to 44 mN m^{-1} as a result of the dissolution of 1-nonanol in water.[42] Since the exact amount of 1-nonanol dissolving into the liquid wall is unknown and there is a paucity of literature for the Gibbs adsorption of water at the 1-nonanol–air interface, we considered a range of plausible values for γ_{oa} and γ_{wa} in the simulation. The interfacial tension γ_{ow} (1-nonanol–water) was determined experimentally to be 8.8 mN m^{-2} and was kept constant for all simulations, since it mutually considers

the Gibbs adsorption. For $\gamma_{ow} + \gamma_{oa} < \gamma_{wa}$, no stable three-phase contact line can be established and 1-nonanol moves over the water wall (Figure 4-i,ii). When the value of γ_{wa} was reduced to 36.43 mN m^{-1} (Figure 4-iii) and 21.86 mN m^{-1} (Figure 4-iv), stable contact lines were observed. As the value γ_{wa} reduces, the 1-nonanol-water interface tilts inward, which is consistent with the experimental observation (Figure 3B). When the value of γ_{oa} is increased from 36.43 to 44 and 51 mN m^{-1} (Figure 4-v–vii) while fixing the values of γ_{wa} and γ_{ow} (44 and 8.8 mN m^{-1}, respectively), stable contact lines are obtained and the 1-nonanol–water interface is gradually tilted inward as well. The simulations based on the phase-field model confirmed the hypothesis, that formation of a stable three-phase contact line and thus liquid wells are possible if the condition, $\gamma_{ow} + \gamma_{oa} > \gamma_{wa}$, is met. When literature values for the surface and interfacial tension (γ_{ow}, γ_{oa}) are contemplated, this is the case for *n*-hexadecane but not for 1-nonanol. However, a variation in the surface tensions at the liquid–air interfaces because of the partial solubility of 1-nonanol with water can enable a transition from an instable to a stable liquid well. This explanation could be applied to other LSTLs, such as toluene or *n*-octane, which fail to fulfill the criterion, $\gamma_{ow} + \gamma_{oa} > \gamma_{wa}$, but nevertheless can be contained by a water well (Figure S4, Supporting Information).[40] Moreover, the specific set of interfacial tensions (γ_{ow}, γ_{oa}, γ_{wa})
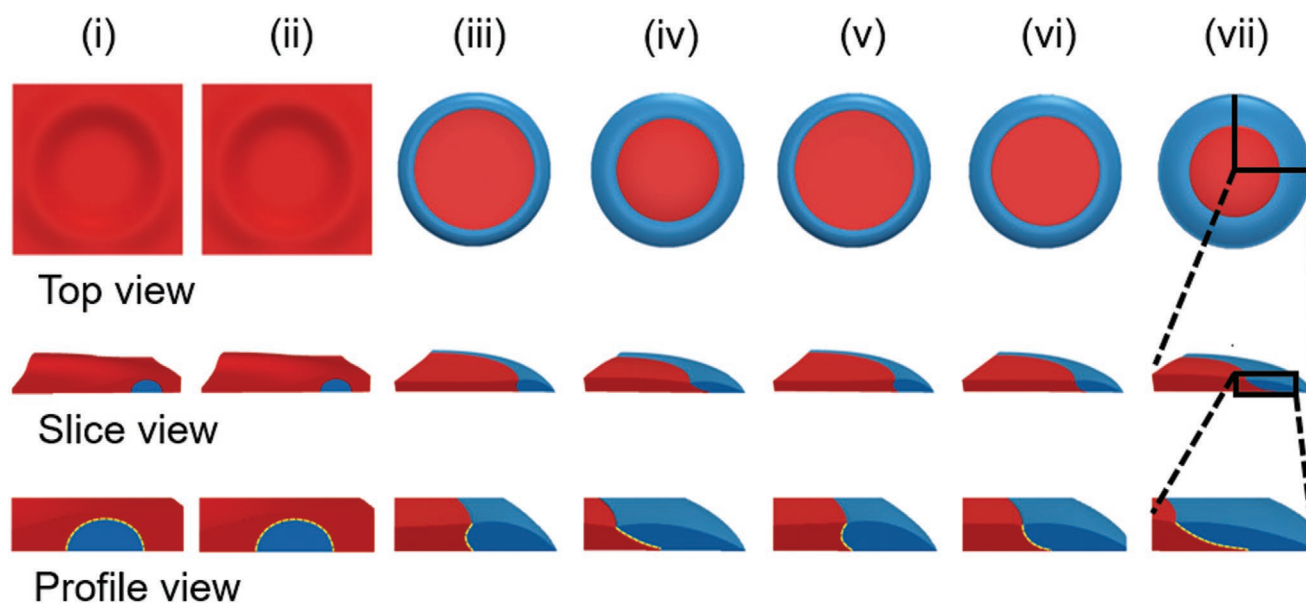
Figure 4. Phase-field simulation for the confinement of 1-nonanol (red) in a ring of water (blue). Each simulation (i-vii) is based on a different set of the surface and interfacial tensions γ_{oa} (organic liquid–air), γ_{ow} (organic liquid–water), and χ_{wa} (water–air). The surface and interfacial tensions (γ_{oa}, γ_{ow}, χ_{wa}) were: i) (28.0, 8.8, 72.86) mN m^{-1},[37,38] ii) (28.0, 8.8, 44) mN m^{-1}, iii) (28.0, 8.8, 36.43) mN m^{-1}, iv) (28.0, 8.8, 21.86) mN m^{-1}, v) (36.43, 8.8, 44) mN m^{-1}, vi) (44, 8.8, 44) mN m^{-1}, and vii) (51, 8.8, 44) mN m^{-1}. The assumed volumes were 100 µL (1-nonanol) and 60 µL (water), respectively. The inner and outer diameters of the hydrophilic surface area are 14 mm and 18 mm, respectively. The first row shows a top view, the second row shows a cross section and the third row highlights the cross section at the interface of 1-nonanol and water.

strongly influences the shape of the organic liquid–water interface, which is most likely the reason for the experimentally observed difference between the shapes of the 1-nonanol–water and the *n*-hexadecane–water interfaces. The sets of surface tensions (Figure 4-iv) (γ_{oa}, γ_{ow}, χ_{wa}) = (28, 8.8, 21.86) mN m^{-1} and (Figure 4-vii) (γ_{oa}, γ_{ow}, χ_{wa}) = (51, 8.8, 44) mN m^{-1} are the most likely possible parameters to reproduce the stable triple junctions of water–1-nonanol–air and water–1-nonanol–substrate, which were observed experimentally (Figure 3B). To support these findings experimentally, a control experiment was performed: A droplet of 1-nonanol deposited on the surface of water formed a droplet instead of spreading over the water surface and forming a wetting layer (Figure S10 and Video S6, Supporting Information). This would not be the case, if literature values for the surface tensions (γ_{oa}, γ_{ow}, χ_{wa}) were contemplated.

To explore potential applications of liquid wells, we used water walls as a recyclable template to structure polymeric materials (**Figure 5**). This process was termed water-templated polymerization (WTP). In a typical WTP procedure, a water wall was formed on a patterned substrate by adding 80 µL of water onto the hydrophilic surface area. Then, a monomer solution consisting of a 4:1 (by weight) mixture of lauryl acrylate (LA) monomer and 1-nonanol, containing 1 mol% of oligo(propylene glycol) dimethacrylate (o(PGDMA)) cross-linker (relative to LA) and 4 wt% Irgacure 379 (relative to LA) photoinitiator was added onto the surface within the water walls (Figure 5A). To initiate the polymerization, the surface was irradiated with UV light (λ_{max} = 365 nm, 17–18 mW cm^{-2}) for 3 min.

After the UV polymerization, the water template was washed away to obtain a free-standing polymer film with a thickness of 150–200 µm (Figure S11, Supporting Information). This WTP process can be used to prepare shaped polymer films in

a single polymerization step (Figure 5B) and is economically and ecologically more efficient than a UV polymerization with a photomask, since all the monomers are polymerized. The removal of a liquid template is very convenient, for example, it can be removed by tilting, rinsing, or evaporation. Finally, the water template can be re-formed by pouring water on the surface. This method could further be interesting for many types of interfacial polymerizations.[43]

3. Conclusion

Water was used as a solid-like wall to contain different liquids in so-called "liquid wells". This was achieved by using hydrophobic–hydrophilic patterns in a core–shell design. The water walls showed to be self-repairing, adaptive, and functional. This unique set of properties arises from the liquid aggregate state of the water walls and can hardly be achieved with solid walls. Drawbacks of liquid wells are the limitations to the height of the water walls and the restriction to low-surface-tension liquids immiscible with water. Liquid wells allow patterning of low-surface-tension liquids in complex 2D shapes with excellent control of the volume and without the need for fluorination, as in the case of superoleophobic or omniphobic patterning strategies. They can further be used as templates to define the shape of a polymer in a process termed "water-templated polymerization" (WTP). The water wall does not attach to the polymer and is easily removed and then re-formed with the same or a different height, which allows fast prototyping of polymer films. Arrays and compartments based on liquid wells are interesting in lab-on-a-chip applications, for example, for on-surface extractions, phase-transfer catalysis, or interfacial reactions. Liquid
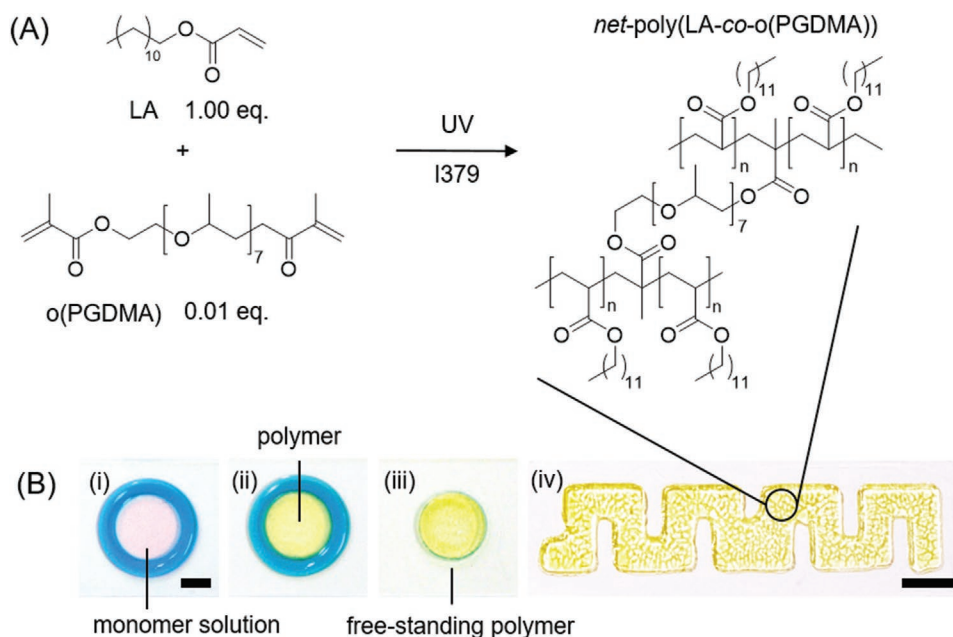
**ADVANCED
SCIENCE NEWS**

www.advancedsciencenews.com

**ADVANCED
MATERIALS**

www.advmat.de

Figure 5. A) Reaction equation of the UV crosslinking polymerization of lauryl acrylate with oligo(propylene glycol) dimethacrylate (o(PGDMA)) using Irgacure 379 as photoinitiator. B) Images showing the process of a water-templated polymerization (WTP). First, i) a liquid well is formed with a monomer solution in the core. Then, ii) the liquid well is irradiated with UV light to trigger polymerization. Lastly, iii) the water walls are rinsed away to reveal the polymer film. iv) Complex shapes can be polymerized in a single step using WTP. Scalebar: 5 mm.

wells can further be useful to study interfacial phenomena such as diffusion or the Marangoni effect, since the liquid–liquid interface can be observed conveniently from the top view using a microscope. More generally, the concept of using water as a recyclable barrier can help to reduce solid waste wherever organic molecules need to be kept separate from each other. Simulation results based on the phase field model suggested that the change in surface tensions at the liquid–air interfaces due to the Gibbs adsorption enables a stable three-phase contact line (air–organic–water). In summary, this report demonstrates a general, fluorine-free, and environmentally friendly approach for the formation of fully liquid, functional, and self-healing compartments for confining and patterning of low-surface-tension liquids.

Supporting Information

Supporting Information is available from the Wiley Online Library or from the author.

Acknowledgements

Conflict of Interest

The authors declare no conflict of interest.

Author Contributions

J.M.S and M.A.K. contributed equally to this work and wrote the paper. J.M.S., P.A.L., and M.A.K. designed the experiments. J.M.S. and P.A.L. proposed the original idea. M.A.K. conducted the experiments. S.H., M.E., Y.W., F.W., B.N. conducted and analyzed the simulation. S.H. helped with Raman experiments.

Data Availability Statement

The data that support the findings of this study are available from the corresponding author upon reasonable request. Higher-resolution versions of the supporting video files are available from the authors under at: https://drive.google.com/file/d/1qwQ4iUvOo6oeOQQcyjLEY5 glwyeuZ6wM/view?usp=sharing.

Keywords

[1] B. Xiong, K. Ren, Y. Shu, Y. Chen, B. Shen, H. Wu, *Adv. Mater.* **2014**, *26*, 5525.

[2] V. Narayanamurthy, Z. E. Jeroish, K. S. Bhuvaneshwari, P. Bayat, R. Premkumar, F. Samsuri, M. M. Yusoff, *RSC Adv.* **2020**, *10*, 11652.

[3] J. J. Heiland, R. Warias, C. Lotter, L. Mauritz, P. J. W. Fuchs, S. Ohla, K. Zeitler, D. Belder, *Lab Chip* **2016**, *17*, 76.

[4] S. Pan, R. Guo, M. Björnmalm, J. J. Richardson, L. Li, C. Peng, N. Bertleff-Zieschang, W. Xu, J. Jiang, F. Caruso, *Nat. Mater.* **2018**, *17*, 1040.

[5] S. S. Latthe, R. S. Sutar, A. K. Bhosale, K. K. Sadasivuni, S. Liu, in *Superhydrophobic Polymer Coatings*, Elsevier, New York **2019**, p. 339.

[6] A. I. Neto, C. R. Correia, C. A. Custódio, J. F. Mano, *Adv. Funct. Mater.* **2014**, *24*, 5096.

[7] H. Cui, W. Wang, L. Shi, W. Song, S. Wang, *Small Methods* **2020**, *4*, 2000573.

[8] M. Benz, M. R. Molla, A. Böser, A. Rosenfeld, P. A. Levkin, *Nat. Commun.* **2019**, *10*, 2879.

[9] H. Wu, X. Chen, X. Gao, M. Zhang, J. Wu, W. Wen, *Anal. Chem.* **2018**, *90*, 4303.

[10] Y. Wang, L. Zhang, J. Wu, M. N. Hedhili, P. Wang, *J. Mater. Chem. A* **2015**, *3*, 18963.

[11] J. Wang, W. Gao, H. Zhang, M. Zou, Y. Chen, Y. Zhao, *Sci. Adv.* **2018**, *4*, eaat7392.

[12] M. Tenjimbayashi, M. Higashi, T. Yamazaki, I. Takenaka, T. Matsubayashi, T. Moriya, M. Komine, R. Yoshikawa, K. Manabe, S. Shiratori, *ACS Appl. Mater. Interfaces* **2017**, *9*, 10371.

[13] L. Ni, C. Dietlin, A. Chemtob, C. Croutxé-Barghorn, J. Brendlé, *Langmuir* **2014**, *30*, 10118.

[14] Y.-K. Lai, Y.-X. Tang, J.-Y. Huang, F. Pan, Z. Chen, K.-Q. Zhang, H. Fuchs, L.-F. Chi, *Sci. Rep.* **2013**, *3*, 3009.

[15] W. Feng, E. Ueda, P. A. Levkin, *Adv. Mater.* **2018**, *30*, 1706111.

[16] M. Benz, A. Asperger, M. Hamester, A. Welle, S. Heissler, P. A. Levkin, *Nat. Commun.* **2020**, *11*, 5391.

[17] M. Cao, D. Guo, C. Yu, K. Li, M. Liu, L. Jiang, *ACS Appl. Mater. Interfaces* **2016**, *8*, 3615.

[18] S. Sett, X. Yan, G. Barac, L. W. Bolton, N. Miljkovic, *ACS Appl. Mater. Interfaces* **2017**, *9*, 36400.

[19] L. A. Thompson, W. S. Darwish, *J. Toxicol.* **2019**, *2019*, 2345283.

[20] X. Chen, G. Wen, Z. Guo, *Mater. Horiz.* **2020**, *7*, 1697.

[21] W. Feng, L. Li, X. Du, A. Welle, P. A. Levkin, *Adv. Mater.* **2016**, *28*, 3202.

[22] S. P. R. Kobaku, A. K. Kota, D. H. Lee, J. M. Mabry, A. Tuteja, *Angew. Chem., Int. Ed.* **2012**, *51*, 10109.

[23] P. Liu, W. He, G. Lu, H. Zhang, Z. Wang, X. Yao, *J. Mater. Chem. A* **2017**, *5*, 16344.

[24] W. S. Y. Wong, *Nano Lett.* **2019**, *19*, 1892.

[25] P. Zhu, T. Kong, X. Tang, L. Wang, *Nat. Commun.* **2017**, *8*, 15823.

[26] J. M. Morrissette, A. Ghosh, R. Campos, J. E. Mates, J. M. Mabry, C. M. Megaridis, *Adv. Mater. Interfaces* **2019**, *6*, 1901105.

[27] V. Jokinen, L. Sainiemi, S. Franssila, *Adv. Mater.* **2008**, *20*, 3453.

[28] V. Jokinen, R. Kostiainen, T. Sikanen, *Adv. Mater.* **2012**, *24*, 6240.

[29] D. Paulssen, W. Feng, I. Pini, P. A. Levkin, *Adv. Mater. Interfaces* **2018**, *5*, 1800852.

[30] J. Forth, X. Liu, J. Hasnain, A. Toor, K. Miszta, S. Shi, P. L. Geissler, T. Emrick, B. A. Helms, T. P. Russell, *Adv. Mater.* **2018**, *30*, 1707603.

[31] E. H. Wong, E. Rondeau, P. Schuetz, J. Cooper-White, *Lab Chip* **2009**, *9*, 2582.

[32] T. S. Kaminski, P. Garstecki, *Chem. Soc. Rev.* **2017**, *46*, 6210.

[33] P. Dunne, T. Adachi, A. Dev, A. Sorrenti, L. Giacchetti, A. Bonnin, C. Bourdon, P. H. Mangin, J. M. D. Coey, B. Doudin, T. M. Hermans, *Nature* **2020**, *581*, 58.

[34] G. V. Kuznetsov, D. V. Feoktistov, E. G. Orlova, S. Y. Misyura, V. S. Morozov, A. G. Islamova, *Int. J. Heat Mass Transfer* **2018**, *126*, 161.

[35] P.-G. de Gennes, F. Brochard-Wyart, D. Quéré, *Capillarity and Wetting Phenomena: Drops, Bubbles, Pearls, Waves*, Springer, New York **2004**.

[36] M. B. Said, M. Selzer, B. Nestler, D. Braun, C. Greiner, H. Garcke, *Langmuir* **2014**, *30*, 4033.

[37] H. Sobol, J. Garfias, J. Keller, *J. Phys. Chem.* **1976**, *80*, 1941.

[38] D. Villers, J. K. Platten, *J. Phys. Chem.* **1988**, *92*, 4023.

[39] A. Estrada-Baltazar, J.d. l. S. López-Lázaro, G. A. Iglesias-Silva, J. Barajas-Fernández, *J. Chem. Thermodyn.* **2020**, *150*, 106225.

[40] A. H. Demond, A. S. Lindner, *Environ. Sci. Technol.* **1993**, *27*, 2318.

[41] R. Stephenson, J. Stuart, *J. Chem. Eng. Data* **1986**, *31*, 56.

[42] Y.-C. Lee, Y.-B. Liou, R. Miller, H.-S. Liu, S.-Y. Lin, *Langmuir* **2002**, *18*, 2686.

[43] F. Zhang, J.-B. Fan, S. Wang, *Angew. Chem., Int. Ed.* **2020**, *59*, 21840.

2100117 (8 of 8)